# Depth-dependent erosion characteristics of marine sediments using a portable erosion flume

**Henning Mohr,**[1] **Samuel Anthony Stanier,**[2] **and David J. White**[3]

[1] Wave Energy Research Centre, The University of Western Australia,
35 Stirling Highway, Crawley, WA 6009, Australia;
E-mail: henning.mohr@uwa.edu.au
Corresponding author.

[2] University of Cambridge, Department of Engineering,
7a JJ Thompson Avenue, Cambridge, CB3 0FA, UK;
E-mail: sas229@cam.ac.uk

[3] University of Southampton,
Boldrewood Innovation Campus, Southampton, SO16 7QF, United Kingdom;
E-mail: david.white@soton.ac.uk

## ABSTRACT

A portable erosion flume has been developed that is capable of estimating erosion threshold and erosion rate relationships for fine-grained specimens over the depth of a typical sample tube. This newly-designed apparatus is a recirculating flume capable of generating steady currents over the exposed section of the sample. In this paper, the erosion properties of two marine sediments have been determined and show a systematic variation with depth by a significant amount. The tests showed that the critical erosion onset velocity doubled over the upper 200 mm of each sample, with the erosion rate falling by an order of magnitude. The increased erosion resistance with depth is consistent with the general trend of erodibility reducing with decreasing moisture content. Ignoring this depth effect when selecting design value of the erosion properties could lead to erroneous predictions of scour rate and extent around subsea structures. As an example, a scour rate prediction beneath a pipeline is conducted, demonstrating the practical value of this technique for determining depth-dependent erosion properties.

## INTRODUCTION

The placement of offshore structures such as subsea cables, pipelines, or foundations on the seabed may result into the removal of sediment due to the amplification of the fluid flow around the structure (i.e. scour). Depending on the magnitude and rate of scour, the stability and integrity of the subsea structure may be compromised, or potentially enhanced. Predictions of the scour process requires the determination of the flow conditions near the seabed and the seabed erosion properties, and is also affected by the shape, size and permeability of the structure.

Seabed erosion properties are well known for uniform sands and predictive formulas for depth and rate of scour have been developed (see for example (Sumer et al., 2002)). However, real marine sediments of a silty nature can have very different erosion properties compared to sands, leading to slower scour development: see for example Kjeldsen et al. (1973), Mohr et al. (2016) or Tom et al. (2016). As shown for example in Roberts et al. (1998) or Mitchener and Torfs (1996), the erosion rates of fine-grained sediments

depend heavily on the bulk sediment properties which may vary spatially. Approaches to assess scour often do not consider the variability of the erosion properties over the potential scour depth, but this variation may be beneficial to the overall stability of the subsea structure.

The aim of this paper is to illustrate the variability of the erosion properties in a soil column by using a newly developed portable flume that is able to test multiple depth layer of a soil sample. The erosion measurements are then related to a typical scour assessment of a subsea structure with a subsequent discussion on the design significance of depth-dependant erosion properties.

## EXPERIMENTAL SETUP

A portable erosion flume was developed for estimating the erosion threshold and erosion rate relationships of fine-grained and coarse-grained sediments. This newly designed apparatus is a recirculating flume capable of generating steady currents over the erosion sample (see Figure 1). It represents an evolution of previous flumes that have been used to study erosion behaviour in situ and in the laboratory, but which did not evolve into tools for routine use in geotechnical site investigation practice (e.g. Young (1977) , Amos et al. (1992), Ravens and Gschwend (1999), Debnath et al. (2007)).

The portable erosion apparatus is 2 m long and 0.5 m wide with a square test section with a cross section of 94 mm by 94 mm and viewing windows. As shown in Figure 1 (a), it is mounted on a 1.5 m high frame allowing the attachment of a 500 mm long soil sample tube below the test section. Using a piston mechanism, the sediment within the sample tube can be pushed into the test section in controlled steps via an opening in the test section bottom. This allows successive testing of the erosion properties of several layers through the depth of the sample.

To produce a steady current, a rim-driven thruster made by Enitech is embedded in the duct of the flume opposite to the test section. As shown in Figure 1 (c), the thruster has its blades mounted on a cylindrical ring which constitutes the rotor of an electric motor. The hubless design offers the advantage of reduced secondary flows (Lee and Chen, 2007; Yakovlev et al., 2011). To further reduce secondary flows, a flow straightener is mounted upstream of the eroding sample with straightening tubes of 6 mm (see Figure 1 (d)).

To measure the total load transport (i.e. both bedload and suspended load transport), a total of 12 acoustic distance sensors are mounted above the erosion sample providing a continuous measurement of the averaged eroding volume over time (see Figure 1 (b)). The 5 MHz acoustic transducer sends and receives acoustic signals and calculates the distance between sensor and reflected object based on the speed of sound in water. The measuring distance of the transducer ranges between 30 mm to 1100 mm exhibiting an accuracy of +/- 0.1 mm and sampling rates of up to 50 Hz. The system is insensitive to small amounts of suspended sediment in the flow compared to conventional measurement methods (e.g. laser scanner). Any erroneous data points due to obstructions in the flow can be filtered because of the high sample frequency and/or the use of blanking distances.

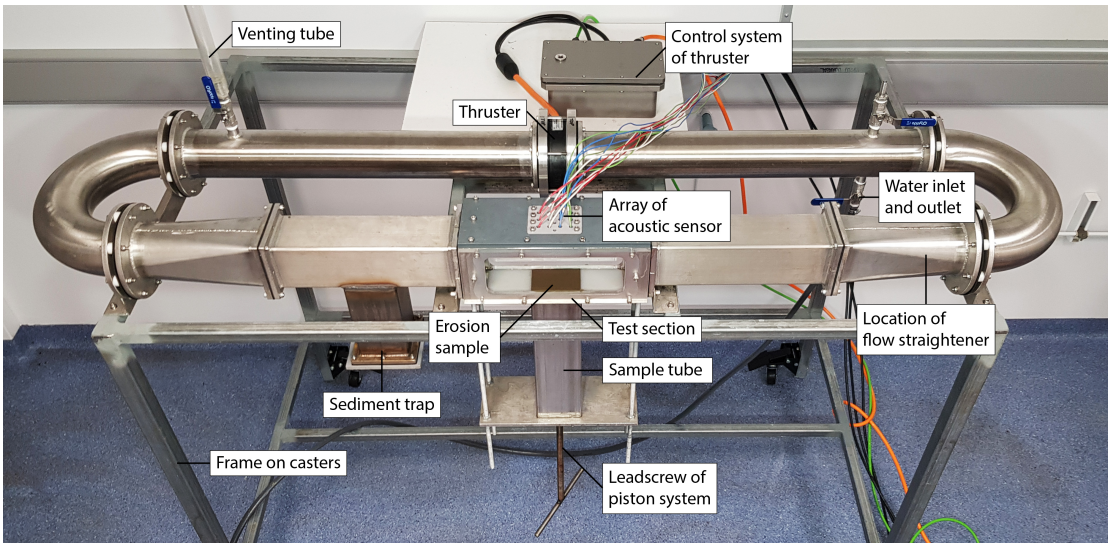


(a) Layout of portable erosion flume.

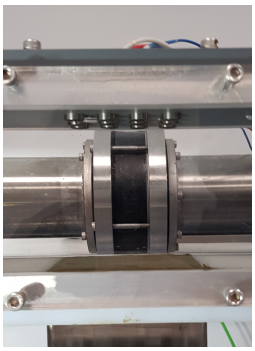

(b) Test-section.

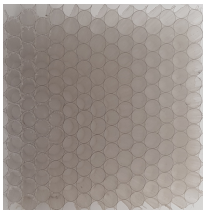

(c) Flow straightener.

(d) Rim-driven thruster.

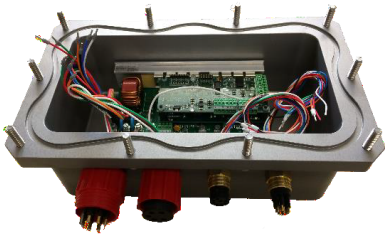

(e) Control system.

Figure 1: Photographs of portable erosion flume and components.

## EXPERIMENTAL PROCEDURE

### Calibration and shear stress determination

Prior to the erosion testing, the flow velocity was measured for different rotational speeds of the thruster. The velocity measurement was performed at 20 mm above the flume bed and in the middle of the working section using a Nortek Vectrino-II Acoustic Doppler Velocimeter (ADV). During erosion testing, the rotational speeds of the thruster were measured continuously and then converted to a velocity based on these initial calibration tests. Figure 2 shows data obtained from this initial calibration.

To convert velocity to shear stress, the velocity measured by the ADV for each rotational speed setting has, therefore, been converted into friction velocity, $u^*$, by solving the following equation numerically

$$U(z) = \frac{u^*}{0.4} \ln\left(\frac{z}{z_0}\right) \ , \tag{1}$$

with the bed roughness length for a hydrodynamically smooth flow

$$z_0 = \frac{\nu}{9u^*} \ , \tag{2}$$

where $U(z)$ is the measured velocity at 20 mm above the bed (i.e. $z$ = 20 mm ), $\nu$ is the viscosity of water (assumed to be 1.003 x $10^{-6}$ m$^2$/s).

The bed shear stress $\tau$ is then given in terms of the friction velocity according to

$$\tau = \rho_{\mathrm{w}} u^{*2} \ , \tag{3}$$

where $\rho_{\mathrm{w}}$ is the density of water (taken as 998 kg/m$^3$). Equations (1) – (3) assume that the velocity profile near the bed is logarithmic, and that the velocity measured at 20 mm above the bed changes little for a given rotational speed setting with the introduction of a soil sample.

### Test procedure

The square sample tube was installed below the test section and pushed using a piston mechanism until the desired depth within the sample for erosion testing was level with the base of the channel. Excess material was carefully removed and the final testing surface gently levelled.

Erosion testing was performed under steady flow conditions. In each test, a steady current velocity (at 20 mm above bed) was introduced starting at $\sim$0.15 m/s for sandy sediments. The water velocity was then increased in $\sim$0.15 m/s increments up to $\sim$2.15 m/s. During each velocity step, the erosion depth was continuously measured at 10 Hz using the array of acoustic sensors system above the sample surface. This allowed for the calculation of the average erosion rate over the sample surface. To avoid edge effects, the averaging was done over a square area which excluded the outer 10% of the sample closest to the boundary (see Figure 3). The erosion rate is defined as the average change in height of the sample (in m) over this area, divided by the time period of testing (in s). For highly erodible flow velocities the tests were run over a shorter time interval.

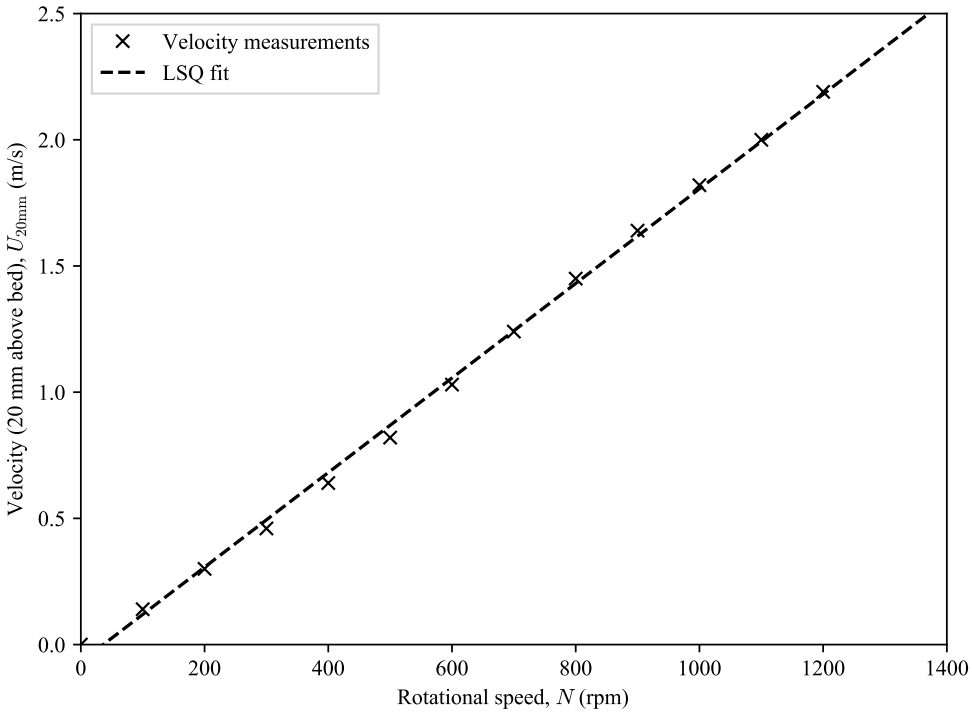


Figure 2: Calibration of flow pump.

The threshold shear stress is defined as the bed shear stress corresponding to significant erosion, which equates to an erosion rate of approximately 3E-7 m/s, or 1 mm/hour. This definition of threshold shear stress leads to an estimate that is solely determined by the measurements and is less subjective than some other definitions (for more information, see Buffington and Montgomery (1997), Roberts et al. (1998), Mohr (2015)). As it is rather difficult to measure a specific erosion rate as low as 3E-7 m/s, the erosion rate measurements have been least squares fitted using the following expression:

$$\eta = M\tau^n \ , \tag{4}$$

where $\eta$ is the erosion rate, $\tau$ is the shear stress, and $M$ & $n$ are fitting parameters. This expression is then used to extrapolate or interpolate to 3E-7 m/s. Equation (4) is a commonly used fit for erosion measurements, see for example Roberts et al. (1998).

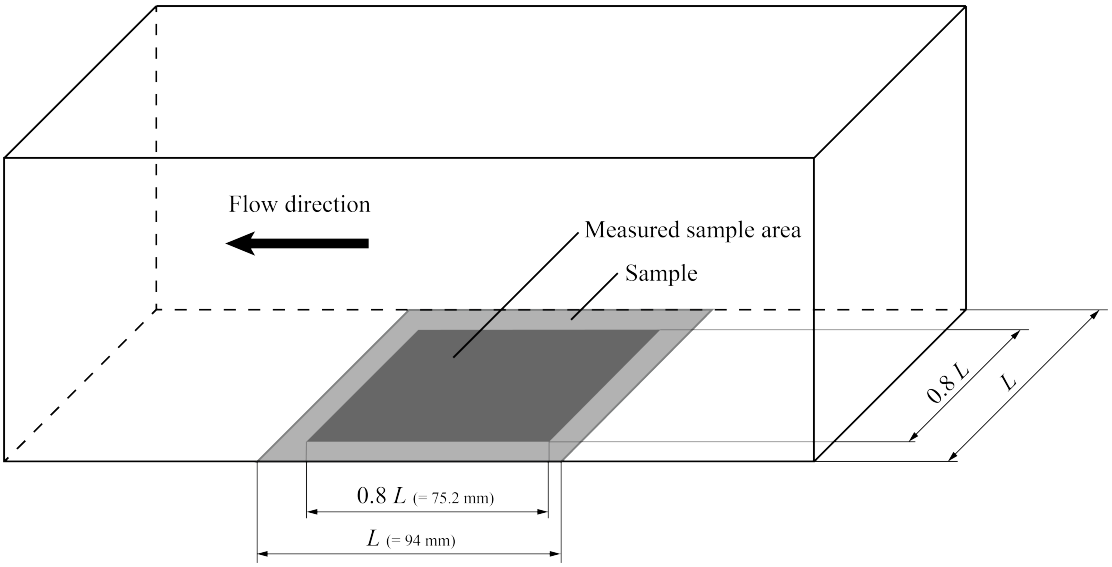


Figure 3: Schematic view of soil sample in working section. $L$ is the length and width of the sample surface.

## EROSION TESTING

Two soil samples, referred to as S1 and S2, were tested for their erosion properties. For both samples, different layers were observed across the tested depth of the square tube by the varying colour and soil consistency during preparation.

Each of the samples could be extruded smoothly into the test section and were prepared carefully. The colour and the grain size of the samples appeared uniform across each tested depth. The soil consistency of S1 compared S2 gave indication of a slightly coarser material, in particular in the top layers. The soil characteristics of these two samples that are used in the calculations to interpret the erosion tests (specifically $d_{50}$ and $G_\mathrm{s}$) are given in Table 1. The median grain size was taken from tests on nearby samples so a possible range of the median grain size is also given and indicated in the figures using error bars or shaded regions.

| Sample | $z$ (m) | $d_{50}$ (mm)* | $d_{50}$ (mm)+ | $G_\mathrm{s}$ (-) |
|---|---|---|---|---|
| S1 | 0 – 0.4 | 0.025* | 0.010 - 0.030+ | 2.67 |
| S2 | 0 – 0.4 | 0.020* | 0.010 - 0.030+ | 2.63 |

* Best estimate based on nearby locations.
+ Range based on nearby locations.

Table 1: Test schedule and properties of sediments tested.

Figure 4 shows the erosion rate measurements for both soil samples for 5 different depth layers (50 mm, 100 mm, 150 mm, 200 mm and 250 mm). The data are fitted using a least squares method to Equation (4). The derived threshold shear stress is determined by the point of intersection between the least squares fit and the threshold

erosion rate of 3E-7 m/s (indicated as a dashed line). The erosion rate decreases with depth (and reducing water content) in both of the samples tested. However, the erosion properties do not correlate with moisture content across the two samples (as presented later).

Table 2 summarises for every erosion test at different depths (i) the water content (by mass), (ii) the threshold velocity at 20 mm above the bed, (iii) the associated threshold shear stress (iv) the threshold Shields parameter and (v) the erosion rate fitting parameters $M$ and $n$ for Equation (4). During testing, erosion patterns across the samples were often intricate. Visual observations of the erosion onset agree reasonably well with the threshold shear stresses determined from the acoustic sensor measurements. In general, close to the threshold shear stress the water became cloudy and very small particles or clumps of particles (approximately 1 mm or smaller in size) were seen to move from the sample surface. As the shear stress increased above threshold the small clumps being removed from the samples increased in size and were observed more frequently.

At the highest shear stress tested, very large clumps were seen to be removed from the samples. These large clumps were removed sporadically and led to the loss of a significant volume of the sample. In other words, the erosion process resembled mass erosion. Zones with increased water content relative to the surrounding material had a tendency to erode sediment in a very short amount of time by mass erosion once the threshold was reached. In these zones of the sample, it appeared that once a particular spot was weakened (for example in the form of an eroding hole), mass erosion started from this spot and propagated along the sample in the streamwise direction. Given the origin of the samples tested, it is possible that these clumps could be burrows (e.g. Kuo and Bolton (2013)).

| Sample | $z$ (m) | $w$ (%) | $U_{\mathrm{cr}}{}^{\mathrm{x}}$ (m/s) | $\tau_{\mathrm{cr}}{}^{+}$ (Pa) | $\theta_{\mathrm{cr}}{}^{+}$ (-) | $M$ ($\mathrm{ms}^{-1}\mathrm{Pa}^{-n}$) | $n$ (-) |
|---|---|---|---|---|---|---|---|
| S1 | 0.05 | 82.57 | 0.78 | 1.29 | 3.16 | 1.46E-07 | 2.8 |
| | 0.1 | 83.80* | 0.78 | 1.29 | 3.16 | 1.63E-07 | 2.38 |
| | 0.15 | 81.65 | 0.96 | 1.88 | 4.6 | 5.54E-08 | 2.67 |
| | 0.2 | 74.71* | 0.98 | 1.92 | 4.7 | 6.97E-08 | 2.23 |
| | 0.25 | 72.35 | 1.32 | 3.34 | 8.17 | 7.00E-08 | 1.21 |
| S2 | 0.05 | 113.35 | 0.91 | 1.7 | 5.33 | 8.05E-08 | 2.47 |
| | 0.1 | 120.16* | 1.18 | 2.71 | 8.49 | 1.30E-08 | 3.15 |
| | 0.15 | 115.76 | 1.51 | 4.27 | 13.38 | 3.84E-09 | 3 |
| | 0.2 | 114.11* | 1.52 | 4.28 | 13.41 | 6.58E-09 | 2.63 |
| | 0.25 | 112.9 | 2.25 | 8.88 | 27.82 | 1.77E-09 | 2.35 |

Table 2: Erosion parameters including threshold velocity at 20 mm above bed and threshold shear stress.

* Water content measurements are interpolated or extrapolated from the moisture content measurements for depths of 0.10 m and 0.20 m (using depths of 0.09 m and 0.19 m, respectively).

+ At $\eta_{cr}$ ∼3e-7 m/s

x 20 mm above bed

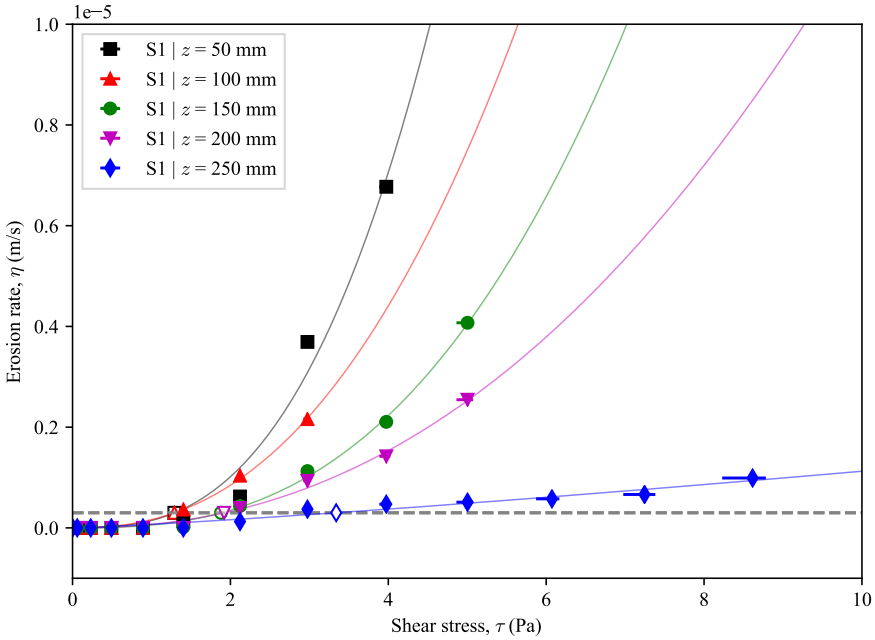


(a)

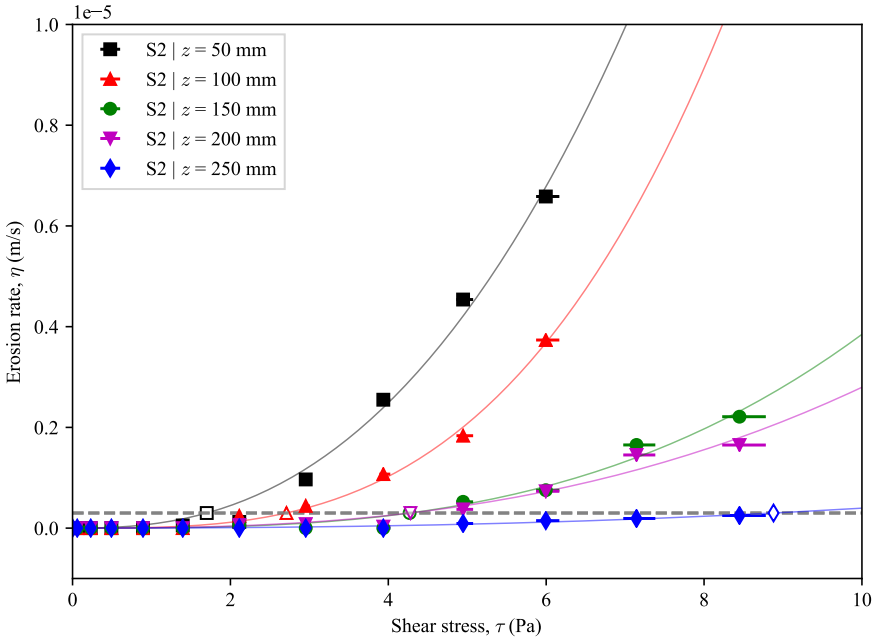


(b)

Figure 4: Summary of erosion data for S1 and S2.

Figure 5 compares the threshold conditions estimated using an empirical formula (known as the Shields curve) in dimensionless and dimensional form. The Shields curve is often assumed to be a good predictor of threshold shear stress for non-cohesive sandy sediments (Soulsby and Whitehouse, 1997). It is evident that for all subsamples the threshold shear stress is higher – by a factor of typically 10 – than that predicted by the Shields curve. The erosion resistance of the material tested is therefore far larger (with 1.3 Pa for the smallest threshold shear stress) than would be predicted assuming a non-cohesive sediment with equivalent median particle size, as would be produced by a prediction using the Shields curve.

The fact that the erosion testing results indicate that the samples tested have higher threshold shear stress than predicted by the Shields curve is in broad agreement with previous measurements obtained from similar sediments (Mohr, 2015). In all of these types of test, surface erosion driven by particle-by-particle movement is difficult to observe with the naked eye due to the small grain sizes, however, mass erosion was certainly observed at higher shear stresses. Threshold shear stresses determined using measured erosion rates based on acoustic distance measurements showed good agreement with visual estimates of threshold shear stress. As shown in Figure 20 and Figure 21, the critical shear stress increases with increasing depth (or reducing water content). There is however no consistent link between moisture content and erosion properties across the two samples. This observation is in agreement with erosion measurements reported by Mohr (2015), who also show that the functional relationship between threshold shear stress and water content is generally different for different sediments.

It is clear from Figure 5 to Figure 7 – which compare samples from a single project location – that erosion properties of these type of natural sediment cannot be reliably estimated solely from geotechnical proxy parameters such as particle size or moisture content. Mohr et al. (2018) show that the most reliable link to a geotechnical property is with permeability, and hypothesise that this is due to the formation of the seepage forces beneath the eroding particles in fine-grained soils. However, they do not follow this observation by recommending to perform laboratory tests to determine permeability as a route to design erosion properties. It is more efficient to use an erosion flume to provide a direct and well-defined basis for selecting design values of erosion properties, as illustrated in this paper.

The deviation of the measured threshold shear stress from the Shields curve is in agreement with previous measurements obtained from similar sediments (Mohr, 2015). Deviations from Shields curve generally occur for finer sediments, for which erosion testing is a more necessary requirement when characterising sediment mobility for design.

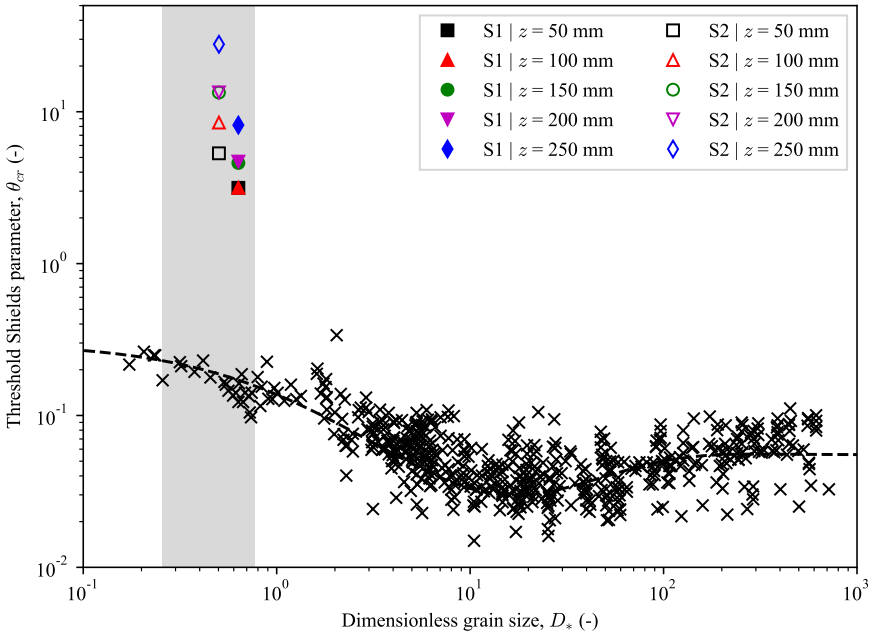


(a)

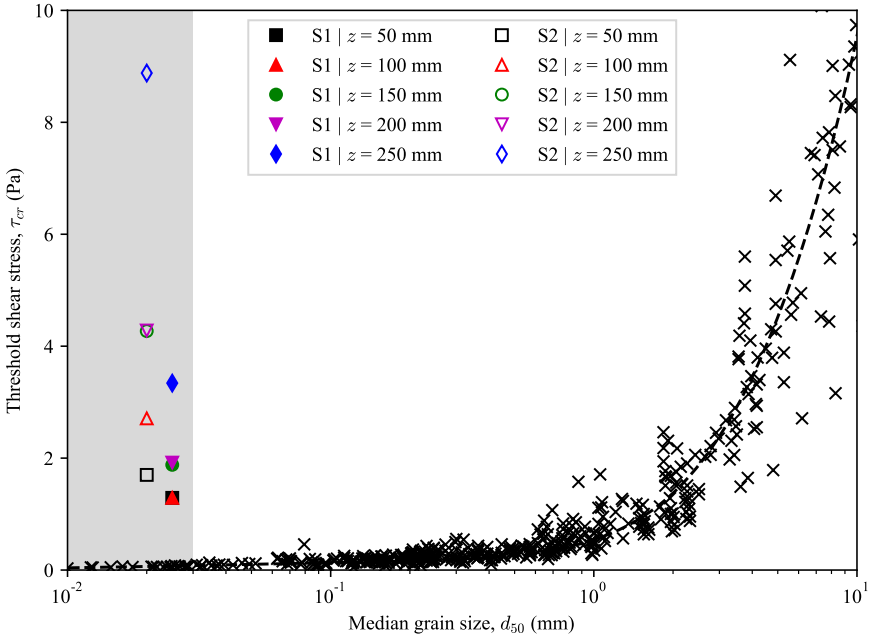


(b)

Figure 5: Comparison of S1 and S2 with Shields curve (a) dimensionless and (b) dimensional. Grey region indicates variability of $d_{50}$ ranging from 0.01 to 0.03 mm.

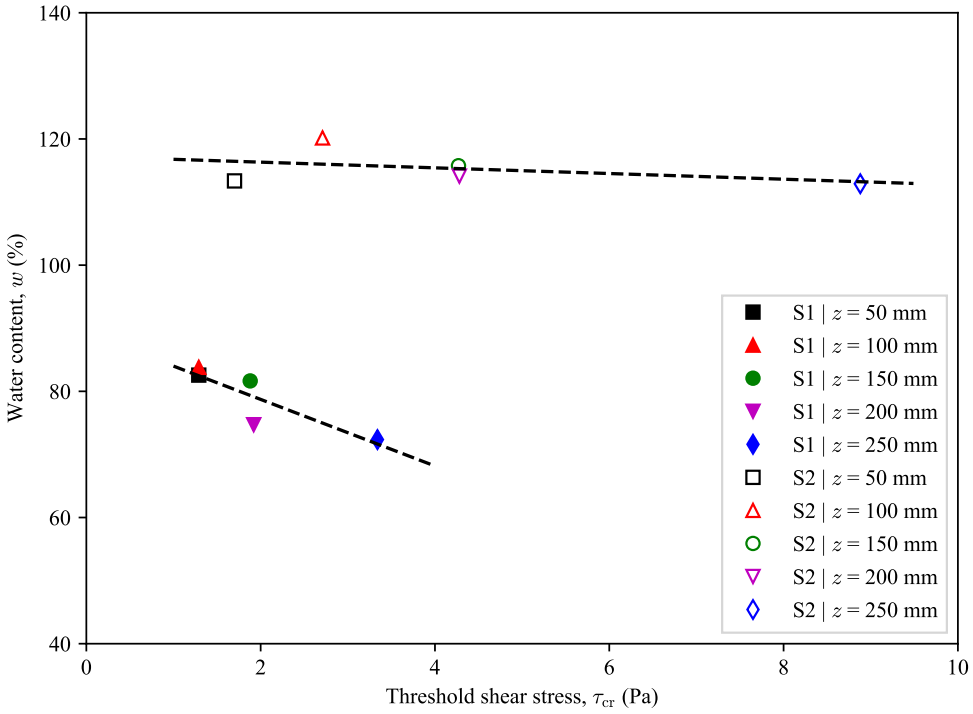


Figure 6: Effect of water content on threshold shear stress for S1 and S2.

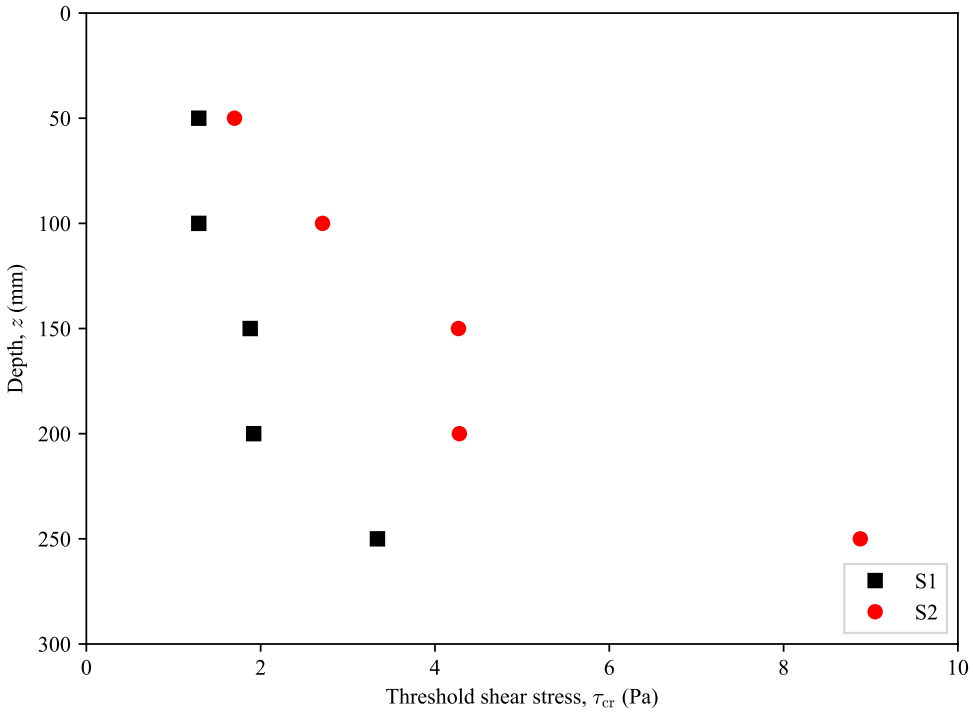


Figure 7: Variation with depth of threshold shear stress for S1 and S2.

## DISCUSSION

The changes of the threshold shear stress and erosion rate with depth have significant implications for the scour assessment of subsea structure and pipelines. These trends with depth affect, in particular, (i) the onset of scour, (ii) the scour hole depth, and (iii) the rate of scour, as discussed below:

- Conventional tests indicate the average erosion characteristics over a sample depth of 200-250 mm (depending on sample length). This may lead to higher threshold and lower erosion rate values compared to measurements from the top layer, if the erosion resistance increases with depth as observed here. The top layer in both samples appeared to be more susceptible to erosion than would be indicated by a single test, performed horizontally in the style adopted in typical erosion tests, where the erosion properties are effectively depth-averaged. For example, the averaged threshold shear stress over a depth from 50 mm to 250 mm (i.e. 200 mm length) for S1 and S2 is 1.94 Pa and 4.37 Pa, respectively. This erosion threshold when averaged over depth are greater compared with the uppermost layer for S1 and S2 by factors of 1.5 and 2.6 respectively.
- The results obtained from the portable erosion flume tests also show that with increasing depth the erosion threshold increases and this, therefore, may affect the progression of a developing scour hole. As a scour hole propagates with depth, it may encounter layers with higher erosion resistance which will limit the development of the scour hole. This is consistent with the observations of Mohr et al. (2016), where it was shown that scour holes depth decreases for finer sediments.
- Pipeline scour experiments performed on sediments from Australia's North West Shelf (NWS) have shown that the scour time scales are proportional to the measured erosion rates (Mohr et al. (2016)). In scenarios where the erosion rate decreases with depth, the scour hole development rate will reduce with the progression of the scour hole depth. The development of the scour hole may even be halted if the deepening of the hole reduces the applied shear stress to below the threshold shear stress .

The implications of the issues outlined above have been illustrated quantitatively using the data from this report in a similar manner to Mohr et al. (2016), using a prediction method for scour hole development beneath a subsea pipeline. Following Mohr et al. (2016), we take a 0.5 m (outside) diameter flowline and consider the implications on the scour hole development predictions of assuming a constant (depth-averaged) and depth-varying erosion rate for the S1 and S2 samples. Assuming that the flowline is subjected to a steady current of 0.8 m/s (referenced at 1 m above the seabed), and rests on a silty seabed ($d_{50}$ = 0.002 mm, comparable to S1 and S2) we calculate a free-field shear stress of 0.67 Pa. The equilibrium scour depth is taken as 60% of the flowline diameter (which is consistent with a large range of experimental results in different sediments; Sumer et al. (2002)) and the shear stress under the pipeline is amplified by a factor of 6 (following Fredsøe and Hansen (1987)). The calculations to predict the evolution of a scour pit beneath the pipeline proceed as follows:

- Assess the amplified shear stress so as to compute the maximum erosion rate.
- Calculate the equilibrium scour depth and the timescales for the fine grained sediment (following Mohr et al. (2016)). To calculate the timescales, two approaches are chosen: (i) averaged erosion rate over 250 mm depth and (ii) changing erosion rate with depth (representative for the portable flume data). Calculation of the different time scales, defined by the parameter $T$, leads to the results in Table 3.
- The timescale parameter $T$ represents the time for the scour hole to develop to 63% of the final value, following an exponential trend with time Mohr et al. (2016).
- The progression of erosion depth with time can then be plotted using relations given in Mohr et al. (2016) and compared for the various scenarios, as shown in Figure 8 for samples S1 and S2.

| ID | No. | Depth (m) | $\tau_{\text{free}}$, $\tau_{\text{amp}}$ (Pa) | $S_{\text{e}}$ (m) | $\eta_{\text{avg}}{}^{*}$ (m/s) | $T_{\text{avg}}{}^{*}$ (s) | $\eta^{+}$ (m/s) | $T^{+}$ (s) [better in days?] |
|---|---|---|---|---|---|---|---|---|
| S1 | 1 | 0.000 – 0.075 | 0.67 & 4.02 | 0.3 | 3.11E-06 | 9.65E+04 | 7.05E-06 | 4.26E+04 |
| | 2 | 0.075 – 0.125 | | | | | 4.41E-06 | 6.80E+04 |
| | 3 | 0.125 – 0.175 | | | | | 2.23E-06 | 1.35E+05 |
| | 4 | 0.175 – 0.225 | | | | | 1.53E-06 | 1.96E+05 |
| | 5 | 0.225 – 0.300 | | | | | 3.73E-07 | 8.04E+05 |
| S2 | 1 | 0.000 – 0.075 | 0.67 & 4.02 | 0.3 | 8.11E-07 | 3.70E+05 | 2.49E-06 | 1.20E+05 |
| | 2 | 0.075 – 0.125 | | | | | 1.03E-06 | 2.91E+05 |
| | 3 | 0.125 – 0.175 | | | | | 2.46E-07 | 1.22E+06 |
| | 4 | 0.175 – 0.225 | | | | | 2.52E-07 | 1.19E+06 |
| | 5 | 0.225 – 0.300 | | | | | 4.60E-08 | 6.52E+06 |

Table 3: Erosion parameter including threshold velocity at 20 mm above bed and threshold shear stress.

$^{*}$ Averaged over depth
$^{+}$ Changing with depth

This calculation shows that the scour development considering different eroding layers is more rapid at shallow depth than the depth-averaged approach, which assumes a higher onset threshold shear stress and lower erosion rate for the surficial material. For the layered approach, as the scour hole progresses, the erosion rate for the presently exposed material is used. This means that as the depth increases the scour development slows down (by more than simply the general exponential decay of scour evolution in uniform material). Eventually, the erosion rate assumed in the depth-averaged approach becomes larger than that measured in the layered testing approach, which would lead to predictions of more rapid and extensive scour hole development than would be observed in reality. The implications of this is that in some instances there is the potential that scour remediation measures might be excessive if depth-averaged measurements alone are relied upon in design. This could have serious cost implications.

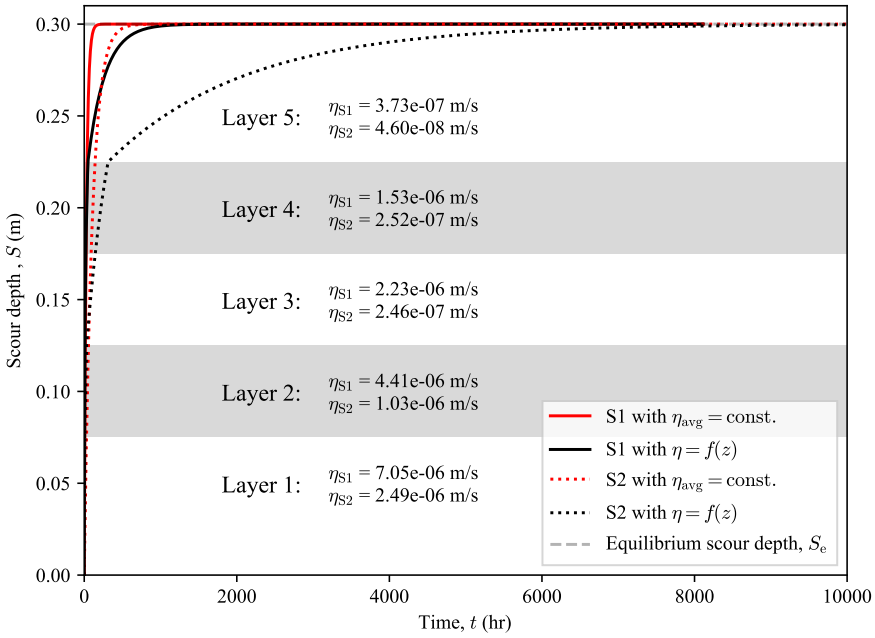


(a)

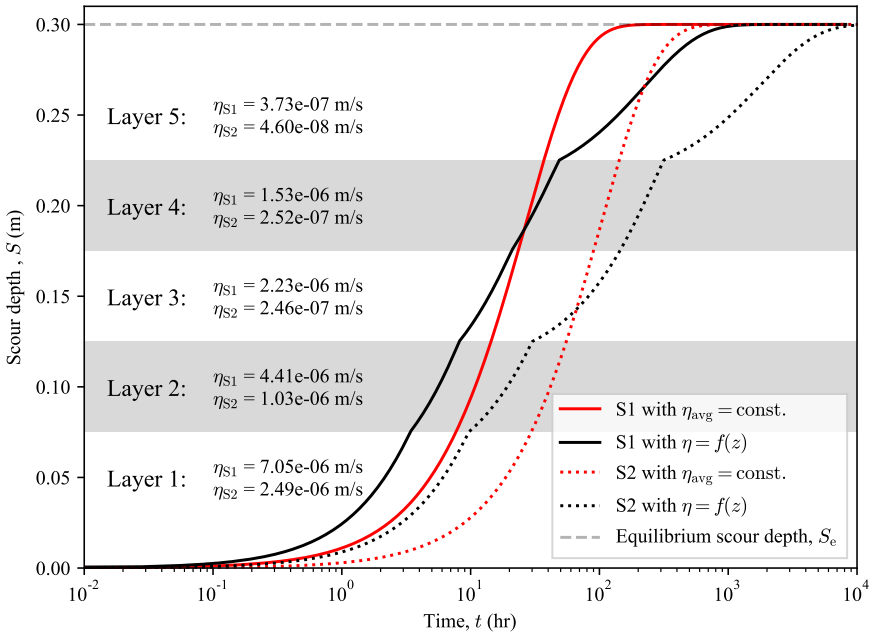


(b)

Figure 8: Pipeline scour predictions using constant or depth varying erosion rates for sample S1 and S2.

For example, if the layered testing approach were to be adopted, the time needed to reach equilibrium would increase from ∼200 hr to ∼1200 hr and ∼700 hr to ∼8000 hr [days better?] for S1 and S2, respectively. This would be particularly important for larger subsea structures where scour hole development would be deeper than measured in these tests, because the influence of changing erosion resistance with depth would be even more important in those scenarios. Eventually, the increase in erosion resistance may even halt the progression of the scour hole development entirely, yet this would not be captured by a single depth-averaged erosion measurement.

## CONCLUSION

Seabed scour can significantly affect the performance and stability of subsea infrastructure in locations with potential sediment mobility. Allowing better predictive tools can mitigate the risk and lead to less cost intensive measures for scour protection.

This paper introduces a newly-developed portable laboratory erosion flume that measures the erosional properties of tube samples in their natural orientation. This allows a depth resolution of the erosion properties so that a depth dependant assessment of scour around subsea structure can be made.

The bulk properties were shown to systematically vary by a significant amount resulting in a increase in threshold shear stress and and a decrease in the rate of erosion which is in line with previous studies (see for more details Whitehouse et al. (2000). The erosion measurements presented in this report show that the erosional properties vary significantly over the uppermost ∼300 mm of the seabed, to a degree that would significantly affect rates of scour propagation. For one sample the critical erosion onset velocity doubled over a 200 mm increase in depth, with the erosion rate falling by an order of magnitude. This is a detail that is not captured by other devices that test a tube sample in a horizontal orientation rather than the natural vertical orientation. Horizontal split samples provide results that effectively average the erosion properties with depth into a single measurement. Such results could lead to erroneous predictions of scour rate. For example, a thin layer with higher erosion resistance could prevent further deepening of a scour feature. However, in conventional split sample erosion tests only the average erosion properties are measured, so effects such as this 'armouring' from a thin layer cannot be detected and used in design. The high resolution with depth is an aspect that can only be explored using the new portable erosion flume.

## ACKNOWLEDGMENTS

This research was conducted by the Wave Energy Research Centre and jointly funded by The University of Western Australia and the Western Australian Government, via the Department of Primary Industries and Regional Development (DPIRD).

## Nomenclature

$\eta$ Erosion rate

$\eta_{\mathrm{avg}}$ Depth-averaged erosion rate

$\nu$ Viscosity

$\rho_{\mathrm{w}}$ Density of water

$\tau$ Bed shear stress

$\tau_{\mathrm{amp}}$ Amplified bed shear stress

$\tau_{\mathrm{cr}}$ Threshold shear stress at an erosion rate of 3E-7 m/s

$\tau_{\mathrm{free}}$ Free field bed shear stress

$\theta_{\mathrm{cr}}$ Dimensionless threshold shear stress at an erosion rate of 3E-7 m/s

$d_{50}$ Median grain size

$G_{\mathrm{s}}$ Specific gravity

$M$ Fitting parameter for Eq. (4) and $n$

$n$ Fitting parameter for Eq. (4)

$S$ Scour depth

$S_{\mathrm{e}}$ Equilibrium scour depth

$t$ Time

$T_{\mathrm{avg}}$ Depth-averaged time scale

$U(z)$ Measured velocity 20 mm above the bed

$u^*$ Friction velocity

$U_{\mathrm{cr}}$ Threshold velocity at an erosion rate of 3E-7 m/s

$w$ Water content

$z$ Depth

## REFERENCES


Amos, C. L., Grant, J., Daborn, G., and Black, K. (1992). "Sea carousel—a benthic, annular flume." *Estuarine, Coastal and Shelf Science*, 34(6), 557–577.

Buffington, J. M. and Montgomery, D. R. (1997). "A systematic analysis of eight decades of incipient motion studies, with special reference to gravel-bedded rivers." *Water Resources Research*, 33(8), 1993–2029.

Debnath, K., Nikora, V., Aberle, J., Westrich, B., and Muste, M. (2007). "Erosion of cohesive sediments: Resuspension, bed load, and erosion patterns from field experiments." *Journal of hydraulic engineering*, 133(5), 508–520.

Fredsøe, J. and Hansen, E. A. (1987). "Lift forces on pipelines in steady flow." *Journal of Waterway, Port, Coastal, and Ocean Engineering*, 113(2), 139–155.

Kjeldsen, S., Gjorsvik, O., Bringaker, K., and Jacobsen, J. (1973). "Local scour near offshore pipelines." *Paper available only as part of the complete Proceedings of the Second International Conference on Port and Ocean Engineering Under Arctic Conditions (POAC), August 27-30, 1973.*

Kuo, M. and Bolton, M. (2013). "The nature and origin of deep ocean clay crust from the gulf of guinea." *Géotechnique*, 63(6), 500–509.

Lee, C. W. and Chen, J. H. (2007). "The characteristics of rim-driven propulsor's flow field." *Proc. 5th International Symposium on Turbulence and Shear Flow Phenomena*, Vol. 2, Munich, Germany, 607–611.

Mitchener, H. and Torfs, H. (1996). "Erosion of mud/sand mixtures." *Coastal engineering*, 29(1-2), 1–25.

Mohr, H. (2015). "Erosion and scour behaviour of marine sediments." Ph.D. thesis, University of Western Australia, Australia.

Mohr, H., Draper, S., White, D. J., and Cheng, L. (2016). "Predicting the rate of scour beneath subsea pipelines in marine sediments under steady flow conditions." *Coastal Engineering*, 110, 111–126.

Mohr, H., Draper, S., White, D. J., and Cheng, L. (2018). "The influence of permeability on the erosion rate of fine-grained marine sediments." *Coastal Engineering*, 140, 124–135.

Ravens, T. M. and Gschwend, P. M. (1999). "Flume measurements of sediment erodibility in boston harbor." *Journal of Hydraulic Engineering*, 125(10), 998–1005.

Roberts, J. D., Jepsen, R., Gotthard, D., and Lick, W. (1998). "Effects of particle size and bulk density on erosion of quartz particles." *Journal of Hydraulic Engineering*, 124(12), 1261–1267.

Soulsby, R. L. and Whitehouse, R. J. S. (1997). "Threshold of sediment motion in coastal environments." *Proc. 13th Australasian Coastal and Ocean Engineering Conference and 6th Australasian Port and Harbour Conference*, 1, 145.

Sumer, B. M. et al. (2002). *The mechanics of scour in the marine environment*. World Scientific.

Tom, J., Draper, S., White, D., O'Neill, M., et al. (2016). "Risk-based assessment of scour around subsea infrastructure." *Offshore Technology Conference*, Offshore Technology Conference.

Whitehouse, R., Soulsby, R., Roberts, W., and Mitchener, H. (2000). *Dynamics of estuarine muds*. Thomas Telford.

Yakovlev, A. Y., Sokolov, M. A., and Marinich, N. V. (2011). "Numerical design and experimental verification of a rim-driven thruster." *Proc. 2nd International Symposium on Marine Propulsors*, Hamburg, Germany, 1–7.

Young, R. A. (1977). "Seaflume: A device for in-situ studies of threshold erosion velocity and erosional behavior of undisturbed marine muds." *Marine Geology*, 23(1-2), M11–M18.